Reaction Path Sampling of the Reaction between Iron(II) and Hydrogen Peroxide in Aqueous Solution

Bernd Ensing and Evert Jan Baerends*

Theoretical Chemistry, Faculty of Sciences, Vrije Universiteit Amsterdam, De Boelelaan 1083, NL-1081 HV Amsterdam, The Netherlands

Received: March 26, 2002; In Final Form: June 18, 2002

Previously, we have studied the coordination and dissociation of hydrogen peroxide with iron(II) in aqueous solution by Car-Parrinello molecular dynamics at room temperature. We presented a few illustrative reaction events, in which the ferryl ion ($[Fe(IV)O]^{2+}$) was formed either by a rebound mechanism or by a two-step mechanism via an iron(IV)dihydroxo intermediate, depending on the starting configuration, which was from either separated reactants or H_2O_2 already coordinated to the Fe^{2+} ion, respectively. In the present work, we test if the illustrative reaction events are indeed representative ones. This is done by generating two sequences of 10 reactive pathways each, using the transition path sampling technique, taking as the initial trajectory the previous reactive pathway which followed the rebound mechanism. Along the generated sequence of reaction pathways, we observed (a) decreasing lifetimes of the intermediate $OH^{\bullet}$ radical, and (b) a change in the reaction mechanism toward the two-step mechanism in which (c) the H-bonded wire through the solvent, along which the $OH^{\bullet}$ radical jumps toward termination, becomes as short as a single H_2O molecule. These trends are rationalized from the point of view that the solvent is not relaxed around the separated reactants in the initial pathway, due to the artificial constraints imposed on the system in order to create a reaction event. During the transition path sampling, the solvent environment relaxes and incorporates H_2O_2 in its hydrogen-bonded network. This leads to fast $OH^{\bullet}$ radical transfer and termination along the established H-bond wires in the solvent, which is in favor of the two-step mechanism.

I. Introduction

Although the strength of molecular dynamics (MD) simulations lies in its use as a statistical tool to compute physical properties as ensemble averages, it is also used to simulate and analyze only single (or very few) illustrative events, for instance to show the possibility of certain chemical reaction pathways (see for some diverse examples refs 1−5). Chemical reactions are commonly activated processes, i.e. the reactants have to pass a free energy barrier (transition state) before transforming into the products. If this reaction barrier is high compared to the thermal energy of the system, the probability becomes very small of finding the reactants in the transition state and thus observe a reaction event on the time scale of the thermal molecular vibrations. In molecular dynamics simulations, which is a good technique to sample the thermal molecular vibrations, the chemical reaction is then a rare event. To simulate a reactive pathway, one therefore has to manipulate the system and enforce a reactive encounter by using for instance a geometric constraint or umbrella potential or by introducing kinetic energy in some translational, rotational, or vibrational mode. Obviously, this manipulation makes the dynamics of the illustrative reaction pathway less realistic. Whether the found pathway is indeed a representative one can be tested using the technique to generate new pathways from earlier found pathways known as the transition path sampling method developed by Bolhuis, Dellago, and Chandler.[6,7] This amounts to making small random changes to the atomic momenta of a randomly chosen configuration along an existing pathway and integrating the equations of motion backward and forward in time from this new point in phase space. If this leads again from reactants to products, it is accepted as a new pathway, which can then again be used to generate new pathways, and so forth.

We have recently studied the dissociation of hydrogen peroxide by iron(II) ions in aqueous solution, using ab initio (DFT) molecular dynamics simulations (AIMD).[8,9] The mixture of Fe^{2+} and H_2O_2, also known as Fenton's reagent,[10] is known to oxidize organic substrates either via $OH^{\bullet}$ radicals[11] or via a high-valent iron oxo species[12] (ferryl ion) as the reactive intermediate. In this previous work, we have generated reactive pathways of the reaction between iron(II) and hydrogen peroxide, starting from two different initial conditions: (a) starting from hydrogen peroxide coordinated to pentaaquairon(II) in water, we found a pathway which resulted in the formation of a dihydroxoiron(IV) moiety, which transformed into the ferryl ion in a second step a short time (3 ps) later; (b) starting from hydrogen peroxide and pentaaquairon(II) separated from each other an arbitrary distance (≈4 Å), we found a pathway which led to the ferryl ion via a more direct rebound mechanism. In both cases, we used bond distance constraints in the initial MD steps to prepare a configuration that would lead to a reactive pathway. Unfortunately, the resulting pathways are likely to contain a memory of the preparation using the unphysical constraints.

In this work, we will apply the transition path sampling technique to generate new reaction paths from the earlier found pathway of the hydrogen peroxide coordinating to and reacting with pentaaquairon(II) in water. In principle, transition path sampling can be (and, in classical MD, has been) used to generate thousands of reaction paths, in which case again the

* Corresponding author.

10.1021/jp025833l CCC: $22.00
Published on Web 07/31/2002

statistical strength of MD is put to good use and quantities such as the reaction rate and rates of energy dissipation can be obtained. Unfortunately at the present time, the computational cost of ab initio molecular dynamics, which is needed to accurately describe the bond-breaking and making and the changing oxidation state of iron during the course of our reaction in water, does not allow for the simulation of more than a few tens of reaction pathways for systems as large as ours (see ref 13 for another example). This should however be enough to obtain reaction paths which have lost the memory of our initial artificial system preparation and show that either or both of the earlier found pathways are indeed realistic illustrative reaction paths or perhaps even reveal a new, third, reaction mechanism.

This article is structured as follows. We begin by giving a short recapitulation of our previous results on the Fenton reaction and our starting reaction pathway in Section II. Then, we briefly summarize the computational details of our Car-Parrinello MD simulations in Section III, followed by an introduction of the transition path sampling technique in Section IV. The results are presented in Section V, starting with the estimation of the transition state of the initial path, following a new procedure. After that, the results of the pathway relaxation are presented in Section V.B. These results, interestingly showing a change in the reaction mechanism, and in fact confirming previous predictions, are rationalized in the discussion part (Section VI), which is followed by the conclusions.

II. Initial Reaction Path

Fenton's reagent, used for oxidation of organic substrates, consists of an aqueous ferrous ion solution which catalyzes oxidation with hydrogen peroxide. The active species is believed to be either the $OH^\bullet$ radical produced via reaction eq 1,[11]

$$Fe^{2+} + H_2O_2 \rightarrow Fe^{3+} + OH^- + OH^\bullet \qquad (1)$$

$$Fe^{2+} + H_2O_2 \rightarrow FeO^{2+} + H_2O \qquad (2)$$

or the ferryl ion (i.e., iron(IV)oxo ion) via reaction eq 2.[12] Static DFT calculations of hydrogen peroxide coordinated to pentaaquairon(II) in vacuo show that the oxygen−oxygen dissociation producing the $OH^\bullet$ radical according to reaction 1 is endothermic by 21 kcal/mol.[9,14] This is, in fact, a reduction of 39 kcal/mol compared to the dissociation of isolated H_2O_2 into two $OH^\bullet$ radicals. The formation of pentaaquairon(IV)oxo and a water molecule according to reaction 2 was proposed to proceed via a dihydroxoiron(IV) intermediate (reaction eq 3)

$$[Fe^{II}(H_2O)_5(H_2O_2)]^{2+} \rightarrow [Fe^{IV}(H_2O)_4(OH)_2]^{2+} + H_2O$$

$$[Fe^{IV}(H_2O)_4(OH)_2]^{2+} \rightarrow [Fe^{IV}(H_2O)_5(O)]^{2+} \qquad (3)$$

and was found to be overall exothermic by 8 kcal/mol. The ferryl ion is 7 kcal/mol lower in energy than its dihydroxo isomer.

Usually, Fenton chemistry takes place in aqueous solution and the solvent effects are expected to play an important role in the reaction mechanisms. The static DFT calculations, for example, pointed out that solvent water molecules can act as bridges in the hydrogen transfer occurring in the second step of reaction 3 and of course also the $OH^\bullet$ radical can jump via solvent water molecules, opening new pathways. The reaction free energy profile of a chemical reaction in aqueous solution can in principle be estimated with ab initio molecular dynamics using an umbrella potential or a geometric constraint (see, for example, refs 15−17) if a good estimate of the transition state and an appropriate reaction coordinate are known. These are, however, not known a priori for our system. To obtain some idea of the possible molecular reaction mechanisms in water, we performed illustrative reaction pathways of the reaction between iron(II) and hydrogen peroxide in water.[8,9] One of the pathways shows a new mechanism, and this pathway will be the initial path for the generation of new pathways in the present study.

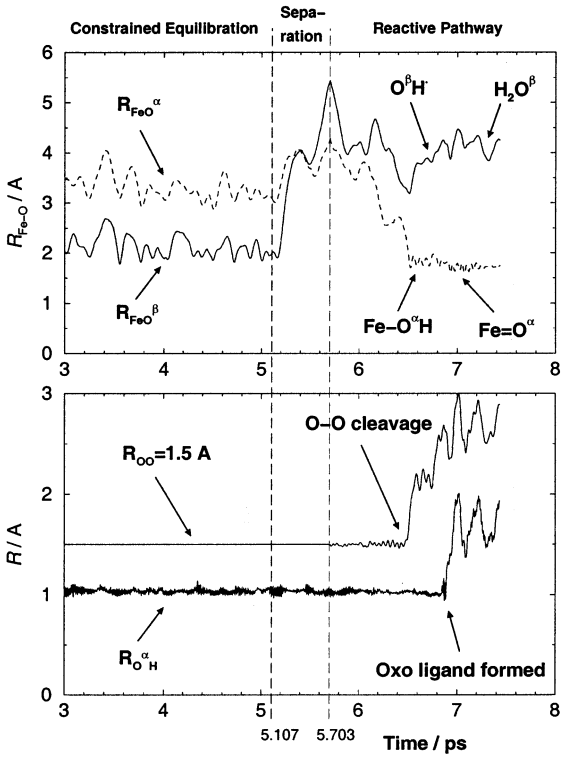

Figure 1. Upper graph: The two Fe−O (H_2O_2 oxygens) distances as a function of time, starting from the last part of the equilibration phase (coordinated Fe−H_2O_2 complex). At $t = 5.1$ ps H_2O_2 is driven away from Fe^{II}. At $t = 5.7$ ps the velocities are reversed. Lower graph: The O−O distance is initially fixed until $t = 5.7$ ps. At $t = 6.5$ ps O−O bond cleavage takes place. The $O^{\alpha}H$ ligand bond is broken at $t = 6.85$ ps, when the $O^{\beta}H^\bullet$ radical grabs the $O^{\alpha}H$ hydrogen.

Figure 1 shows characteristics of the pathway of ref 9 that will be used as the initial pathway for the transition path sampling that we will carry out in the present work. The relevant geometric parameters (the FeO^{α} and FeO^{β} distances in the upper graph and the hydrogen peroxide $O^{\alpha}O^{\beta}$ and $O^{\alpha}H$ distances in the lower graphs, O^{α} and O^{β} being the H_2O_2 oxygens with O^{α} the one that becomes connected to iron in the reactive pathway) are shown as a function of time for this pathway. The actual reaction pathway starts at a time $t = 5.7$ ps denoted by one of the vertical dashed lines. Everything before that time will be regarded as the preparation for this pathway. The first 5 ps are merely equilibration of the system, which consists of hydrogen peroxide coordinated to pentaaquairon(II) and 26 solvent water molecules. The cubic unit cell was subject to periodic boundary conditions and a Nosé thermostat maintained an average temperature of $T = 300$ K. To avoid a premature breakup of the complex, the H_2O_2 oxygen−oxygen bond distance was constrained to 1.5 Å. At $t = 5.1$ ps, indicated by the first vertical dashed line, we constrained the five FeO bond distances between the iron ion and the water ligands and decreased them from the average $R_{OO} = 2.1$ Å to $R_{OO} = 1.8$ Å in 100 AIMD steps, which forces the sixth ligand, H_2O_2, out of the coordination shell. At

$t = 5.7$ ps, we have arrived at a configuration with pentaaquairon(II) (with a vacant coordination site) and hydrogen peroxide separated from each other by a little more than 4 Å with a set of atomic momenta that will lead to further separation. This configuration we take as the starting point for our reaction pathway and we reverse all atomic velocities to obtain a set of momenta that will lead to approaching reactants. Also, the velocities of the fictitious plane wave coefficient dynamics are reversed as well as the velocity of the Nosé thermostat variable. Here our reaction pathway starts, with now atomic velocities that will lead to approaching reactants.

The simulation was now continued without the bond distance constraints. Due to this difference with the separation process, the system initially tracks back onto the trajectory before the velocities were reversed, but soon diverges from it strongly, finding a new route which leads to coordination of H_2O_2 to the iron complex. Indeed, at $t = 6.5$ ps, the hydrogen peroxide coordinates again to the iron complex, but bonds now with the other oxygen, denoted O^{α}, to iron (see again Figure 1). As soon as H_2O_2 coordinates to the complex, O−O lysis takes place, and an iron(III)hydroxo moiety is formed together with an $OH^{\bullet}$ radical. At about $t = 6.9$ ps, the $OH^{\bullet}$ radical grabs the Fe(III)−OH hydrogen to form a water molecule and the ferryl ion.

The mechanism followed by this pathway will be referred to as the rebound mechanism, because the $OH^{\bullet}$ radical that splits off in the O−O lysis step rebounds to abstract the hydrogen from the hydroxo ligand. The rebound mechanism differs from pathways in which the $OH^{\bullet}$ radical shunts, via a H-bond wire of solvent water molecules, to a terminating water ligand, which was observed when starting from hydrogen peroxide coordinated to pentaaquairon(II) in water.[8] In the latter case, a dihydroxoiron(IV) species was formed (much as predicted by the DFT calculations of the complex in vacuo), which transformed via proton exchange with the solvent into the ferryl ion a few picoseconds later. We will refer to this mechanism as the two-step mechanism. The main question that remains concerning the rebound pathway is: to what extent is the found reaction pathway dictated by the manipulation at time $t = 5.1$ ps, and is it thus a representative pathway? We attempt to answer this question by applying the transition path sampling method to generate pathways that will have no memory of this preparation strategy.

III. Computational Details

The microscopic reaction pathways presented in this paper were computed using the Car-Parrinello method.[18] This method combines classical molecular dynamics (MD) with a quantum mechanical computation of the electronic structure. The forces on the nuclei are obtained from the electronic ground-state energy, rather than from an empirical force field, which is why Car-Parrinello MD often is referred to as ab initio molecular dynamics (AIMD). The Car-Parrinello technique differs from other AIMD methods by the dynamical optimization method, known as simulated annealing, for the electronic wave function degrees of freedom (i.e., the basis set expansion coefficients) which can be treated simultaneously with, and on the same footing as, the Newtonian nuclear dynamics. The parameter of inertia, usually called "fictitious electronic mass", controlling the response of the basis set coefficients to the potential in the simulated annealing approach, is chosen much smaller than the atomic masses. This way, the wave function adapts instantaneously to the moving nuclei, keeping the electrons sufficiently close to the correct ground state. The Verlet algorithm is used to integrate the equations of motion for the nuclear dynamics and for the coefficient optimization. In the present work, the fictitious electron mass was chosen 500 au ($\approx 4.555 \times 10^{-28}$ kg), which limits the time step to 0.145 fs.

TABLE 1: Bond Dissociation Energies and Rearrangement Energies in kcal/mol for Isolated ("gas-phase") Complexes, Calculated with the Amsterdam Density Functional Program (ADF) and the CP-PAW Program Using the Becke-Perdew Exchange Correlation Functional

gas-phase reaction	CP-PAW	ADF	$\Delta\Delta E$
A $[(H_2O)_6Fe^{II}]^{2+} \rightarrow [(H_2O)_5Fe^{II}]^{2+} + H_2O$	22.1	21.7	0.4
B $[(H_2O)_6Fe^{II}]^{2+} \rightarrow [(H_2O)_5Fe^{II}]^{2+} - H_2O$	−2.3	−3.5	1.2
C $[Fe^{II}(H_2O)_5]^{2+} + H_2O_2 \rightarrow [Fe^{III}(H_2O)_5OH]^{2+} + OH^{\bullet}$	−8.4	−2.1	−6.3
D $[Fe^{III}(H_2O)_5OH]^{2+} + OH \rightarrow [Fe^{IV}(H_2O)_5O]^{2+} + H_2O$	−30.8	−28.7	−2.1

The electronic structure is calculated with density functional theory (DFT).[19] We used the Becke-88[20] and Perdew-86[21] gradient corrected functionals for exchange and electron correlation, respectively. The Car-Parrinello simulations were performed using the CP-PAW program developed by Blöchl,[22] who integrated the projector augmented wave (PAW) method with the ab initio molecular dynamics. The PAW method uses an augmented plane-wave basis for the electronic valence wave functions and, in the current implementation, frozen atomic wave functions for the core states. The plane-wave basis expansion was cut off after functions with a kinetic energy of 30 Ry. The 1s electrons of oxygen and up to the 3p electrons for iron were kept frozen. For the augmentation for H and O, one projector function per angular momentum quantum number was used for *s*- and *p*-angular momenta. For Fe, one projector function was used for *s*- and *p*- and two for *d*-angular momenta.

The advantage of PAW over the more commonly used pseudopotential approach is that transferability problems should be largely avoided. However, as with all methods in which the core is represented approximately, there will be some loss of accuracy. Extensive tests are therefore required and we have previously shown that bond energies and geometries of small molecules and complexes computed with CP−PAW agree very well with highly accurate all-electron DFT results obtained with the ADF[23] program.[15] However, we have in the course of the present work noted that reaction energies of chemical reactions involving a change in the formal oxidation state of iron sometimes exhibit relatively large (several kcal/mol) discrepancies with accurate (large basis set, all-electron) ADF calculations. Table 1 shows four reaction energies of gas-phase reactions involving simple aqua iron complexes, calculated with CP-PAW and with ADF. The same exchange-correlation functional was used in both calculations. The Kohn-Sham orbitals were expanded in the ADF calculation in a large even-tempered all-electron Slater-type basis set containing: 4s, 2p, and 1d functions for hydrogen; 6s, 4p, 2d, and 1f functions for oxygen; and 11s, 7p, 5d, and 1f functions for iron.[24] The CP-PAW calculation used plane-waves with a cutoff of 30 Rydberg. Reactions A and B, show the typical small differences in the order of 1 kcal/mol due to the differences in basis set and the frozen core approximation used with PAW. However, reactions C and D, which involve a change in the iron oxidation state, show larger discrepancies, up to 6.3 kcal/mol for the reaction in which iron(II) is oxidized to iron(III). The error does not seem to be due to the plane-wave cutoff of 30 Ry (it is not reduced when going to 50 Ry) and can be attributed to the partial waves for the inner region of the valence electrons and the projector functions used in the PAW calculations. The purpose of the present work is the application of transition path sampling in order to obtain reaction pathways which have lost the memory of their initial artificial construction. This memory effect, as

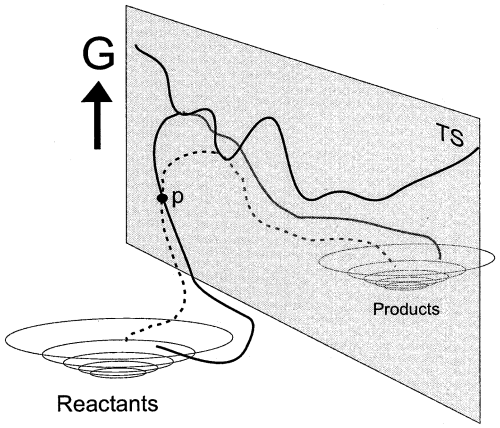

Figure 2. Schematic representation of the free energy landscape with two stable, attractive wells separated by a transition state ridge, which connects the highest free energy points of all possible paths connecting the reactant and product states. The dotted line represents a new trajectory that was branched off at point *p* from an old trajectory (bold line) and surpasses the TS ridge at a lower point.

we will see, is related to the solvent motion and the formation and breaking of H-bond networks in the solvent, which are well represented by the present type of CPMD simulations, as demonstrated earlier.[15] We therefore feel that the present CPMD method can be applied to this type of study, but we have to take the limitations due to the limited accuracy of the reaction energetics in mind; obviously one cannot realistically calculate a reaction rate with this type of CP-PAW calculation for a reaction involving change of oxidation state of Fe.

For the AIMD simulations of the Fenton reaction in aqueous solution in this paper, we applied periodic boundary conditions to a cubic box with an edge of 9.900 Å, containing one iron ion, one hydrogen peroxide molecule, and 31 water molecules. The positive 2+ charge of this system was compensated by a uniformly distributed counter charge. In the reaction path sampling technique, we quenched the fictitious basis set coefficient dynamics after every fourth reaction pathway generation, to avoid deviations from the Born-Oppenheimer surface. A Nosé thermostat[25] maintained a constant temperature of $T = 300$ K.

IV. Transition Path Sampling

The technical details of transition path sampling and its potential to study the dynamics of rare events are described in a number of interesting papers by Bolhuis, Dellago, Geisler, and Chandler.[6,7,26] The part that we are interested in, namely, the generation and relaxation of reaction pathways, is schematically illustrated in Figure 2.

In the rugged multidimensional free energy landscape, we find two stable states: the reactant state and the product state, which are separated from each other by an irregular energy barrier depicted by the line in the plane in Figure 2. This line, in fact, connects all highest points of all the possible (reaction) pathways from the reactant state to the product state. We can define the transition path ensemble as the ensemble of all possible trajectories connecting the two stable states, within a certain finite time. The two stable states can be regarded as basins of attraction so that an MD simulation of the system started from a configuration in the neighborhood of one of the stable states is very likely to sample only this stable state region and will not be seen to cross the barrier to the other stable state, unless we simulate for a very long time. Crossing the barrier ridge is of course more probable through a low-lying pass than via some high top on the ridge. However, if we manage to find a connecting pathway over the barrier by some artificial manipulation of the system (as we did for the hydrogen peroxide iron(II) complex, by first driving out H_2O_2 from the coordination shell), we are likely to find a too-high barrier crossing point. Such an initial pathway is depicted in Figure 2 by the solid line from the reactant state to the product state. If the found pathway is indeed not a physically probable transition path, we can *relax* within the transition path ensemble from the improbable pathway to more probable paths by generating new pathways from our initial path. We therefore randomly pick a point *p* on the initial pathway, from where we branch off a new pathway, by making small random changes in the atomic momenta. Integration of the equations of motion forward and backward in time might result in a new pathway (called a new *generation*), represented by the dashed line. On this pathway, we can again randomly pick a new point *p* and again generate a trial pathway, et cetera. If the new trial pathway does not connect the two stable states (within some arbitrarily chosen finite time span), but instead remains in one of the stable states, we do not accept the new pathway but repeat the procedure starting from another point on the previous pathway. Success or failure of the pathway generation procedure depends on the following points: (1) the smaller the random changes of the atomic momenta, the larger the probability to succeed in finding a new reaction path; (2) the closer point *p* is located to the ridge of the barrier tops, the larger the probability of succeeding in finding a new reaction path.

On the other hand, the smaller the random changes of the atomic momenta the more the new pathway will follow the previous pathway, and the more pathways we have to generate in order to arrive at pathways which have no memory of the initial pathway. The magnitude of the momentum changes is thus a compromise, and we should therefore not strive for a 100% success rate in the pathway generation procedure. Dellago et al. have carried out a thorough efficiency analysis for a simple model system, finding that an acceptance probability in the range of 30−60% yields optimum efficiency.[27]

We want to make two more remarks on Figure 2. First, it is possible that there exists more than one reaction "channel" separated from each other by an energy barrier. In Figure 2, this is illustrated by the bump in the middle of the transition ridge, with lower lying passes on both sides (which even might lead to two different stable product states). Although in principle also pathways might be generated from the drawn pathway which pass through the right-hand-side channel, the chances of that become smaller as the separating bump increases. In practice another artificially initiated pathway would be needed as a starting point for the sampling of pathways through this second channel. The second remark regards the new definition of transition states within this theory. Instead of one transition state (TS) based on the intrinsic (zero Kelvin) reaction coordinate, an ensemble of transition states can be defined of all possible reaction pathways. The TS of each generated pathway is found by branching off a large number of new trajectories from a point *p* on the given pathway, starting with random momenta. From a point *p* close to one of the stable states most or even all trajectories will end up in the stable state. On the TS ridge, however, the chances are fifty-fifty to go either way, so that a point *p* from which half of the generated trajectories end up in each of the stable states can be identified as a point on the TS ridge. Of course, this TS point does not have to be connected to the highest potential energy along the pathway, since the TS is determined not only by the energy but also by the entropy.

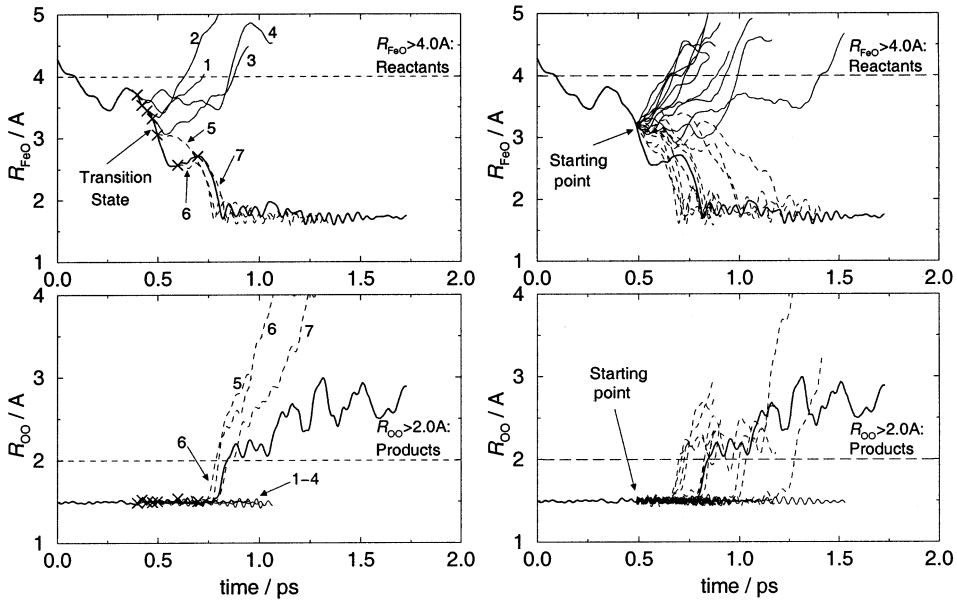

Figure 3. Left-hand-side: estimation of the position of the transition state on the reaction path (bold line) by starting new trajectories from certain configurations (denoted with crosses) with zero velocities. Solid lines indicate trajectories which recross back to the reactant state; dashed lines are paths which lead to oxygen−oxygen lysis (products). Right-hand-side: testing the TS position estimate by initiating 20 trajectories with random velocities, starting between points 4 and 5 of the left-hand-side trajectories. Indeed, half of them end up in the reactant state, and half in the product state.

In particular, the potential energy along the pathway exhibits thermal fluctuation, which makes the maximum potential energy along the path a less useful parameter. We are, for example, not interested in the highest potential energy point if that high energy arises from motion (collision) of solvent molecules somewhere far from the reactants in the box. The TS point on a certain pathway should be a point on the *free energy* TS ridge. Having determined the TS points for a very large number (say, one thousand) of paths, interesting properties of the transition state ensemble (i.e., the ridge in Figure 2) can be studied, such as the average solvent coordination in the transition state configurations.[26]

In the next section, we will first attempt to find the transition state for our initial pathway for the reaction between pentaaquairon(II) and hydrogen peroxide in water. Next we will use the transition path sampling technique to generate new pathways.

V. Results

A. Determination of the Transition State on the Initial Reaction Path. In the original transition path sampling procedure, to determine the transition state of a single reaction pathway, a large number of trajectories have to be initiated with random initial atomic velocities from some trial point along the pathway. From the ratio of the number of trajectories that end in the reactant well and the number of trajectories that end in the product well, it can be determined whether the trial point is located on the reactant side or the product side of the TS point. If more than 50% of the trajectories ended in the reactant well, a new trial point is chosen located at the product side of the previous point (and vice versa), and this procedure is repeated until the TS point is found for which 50% of the trajectories generated from this point end up in the reactant well and 50% end up in the product well. Unfortunately, this technique is computationally very expensive in combination with Car-Parrinello MD for our system. Therefore, we introduce an alternative strategy to speed up the search for the TS point. Instead of branching off many trajectories from a trial point with random initial atomic velocities, we start one trajectory with zero atomic velocities. The initial direction of the system is therefore determined by the potential energy rather than the free energy, as was the case in the original strategy. If the system ends up in the reactant state, we try a new trial point located more to the products side along the pathway and vice versa. Due to the low temperature the system will have (starting from zero Kelvin) and since mainly the starting direction of the generated trajectory is relevant, a damped Nosé thermostat which heats the system to $T = 300$ K is used to accelerate the search even more. Since we are however interested in the free energy transition state position, we will in the end nevertheless use the original generation procedure to find the exact location, but our "0 Kelvin" approach provides a very cheap means to obtain a good first guess for the expensive full procedure.

The left-hand-side graphs in Figure 3, show the result of our "0 Kelvin" approach to narrow down the TS position on our initial pathway, defined in Section II, of the reaction between pentaaquairon(II) and hydrogen peroxide in water. Note that the starting point of our initial path at $t = 5.703$ ps in Figure 1 has been set to $t = 0$ in Figure 3. The upper left-hand-side graph shows again the iron(II)−oxygen distance (bold line), which equals $R_{FeO} = 4.3$ Å at the start at $t = 0$ and decreases to $R_{FeO} = 1.9$ Å 800 fs later, as hydrogen peroxide coordinates and bonds to iron and the oxygen−oxygen bond breaks (which is shown in the lower graph). The horizontal dashed lines depict our choice for the order parameters that define the stable states. That is, for $R_{FeO^{\alpha}} > 4.0$ Å the system finds itself in the reactant well of separated iron(II) and hydrogen peroxide, and for $R_{OO} > 2.0$ Å the system finds itself in the product well of dissociated hydrogen peroxide. Note that this definition imposes no constraints—the final product may consist of the $OH^{\bullet}$ radical, a dihydroxo or oxo iron complex, or something we had not thought of yet.

The crosses on the bold line in both of the left-hand-side graphs denote the trial points, from which trajectories were started with zero velocities. We see that the trajectories originating from the first four trial points all end up in the

reactant well of $R_{FeO} > 4.0$ Å (solid lines). The trajectories of the next three points all end up in the product state of $R_{OO} > 2.0$ Å (dashed lines). We have thus narrowed down the estimate for the TS location between the fourth point at $t = 0.473$ ps ($R_{FeO} = 3.3$ Å) and the fifth point at $t = 0.498$ ps ($R_{FeO} = 3.1$ Å).

To verify this estimate of the TS location, we started 20 AIMD trajectories at the point at $t = 0.485$ ps (in the middle between points 4 and 5) where the iron−oxygen separation is $R_{FeO} = 3.21$ Å. The initial atomic momenta were drawn from a Gaussian (Boltzmann) distribution of a temperature of $T = 300$ K and corrected for any total momentum of the system. In the right-hand-side graphs of Figure 3, the 20 trajectories have been plotted. Ten of them end up in the reactant well and the other 10 end up in the product well. Perhaps a little fortuitously, apparently our approach resulted in a very good estimate of the transition state location on our reaction pathway, which could indicate that the TS point on the free energy surface (sampled by the original method, starting with random momenta) is not very different from the TS point on the potential energy surface (which determines the TS position resulting from our "0 Kelvin" approach).

The large iron−oxygen separation of $R_{FeO} = 3.21$ Å and the unchanged O−O distance in the transition state configuration indicates that the barrier is mainly determined by the solvent environment for our reaction pathway and not by the actual oxygen−oxygen lysis. Earlier, we had inferred that this barrier for hydrogen peroxide coordinated to iron(II) in aqueous solution must be small in the PAW calculation as we observed the spontaneous reaction to the ferryl ion or to an iron(IV)dihydroxo complex, during AIMD simulations.[15,8] Also in the present simulation the barrier for O−O bond breaking is apparently small. It is possible that the barrier is underestimated in the PAW calculation, in view of the overestimation of higher oxidation states for iron as mentioned earlier in Section III. In ADF calculations (STO basis functions) for the isolated complex we have found a barrier, although a small one (6 kcal/mol), for the O−O lysis of the coordinated hydrogen peroxide in the pentaaquairon−hydrogen peroxide complex. The TS barrier in this case was found when the leaving $O^{\beta}H$ radical was in the process of forming a bond to a H atom of an adjacent ligand, the calculations in vacuo preventing it from going into solution.[14] The TS position found in the present CPMD simulation in solution is clearly connected to a barrier in the ligand coordination process. This can be understood assuming that the approaching hydrogen peroxide has to break (partially) with the energetically favorable solvation shell before it can form an energetically favorable bond with the iron complex. The correspondence between the methods to estimate the TS position (namely "random momenta" and "0-Kelvin") can be understood in the same way when we also assume that the entropy loss due to coordination is less important. For comparison, the free energy barrier for exchange of a water molecule from the first coordination shell of iron(II) in water was estimated to be 8.6 kcal/mol with NMR spectroscopy, which is indeed mainly energetic ($\Delta H^{\ddagger} = 7.7$ kcal/mol, $-T\Delta S^{\ddagger} = 0.9$ kcal/mol).[28]

B. Transition Path Sampling. In this section, new reactive pathways for the O−O bond breaking upon coordination of an hydrogen peroxide molecule to an iron(II) ion in aqueous solution will be generated, using the transition path sampling technique. To this end, a point on an existing reaction pathway has to be chosen as the starting configuration of a new pathway. In the present sampling procedure, a configuration file with the atomic configurations and wave function coefficients was saved every 1000 time steps (145 fs). One of the saved configurations was randomly chosen as the starting point for a new pathway. The first new successful reaction path initiated from a point on our initial pathway, will be referred to as the first generation path; a successful reaction path initiated from a point on this first generation path makes then a second generation path, et cetera. A *sequence* of reactive pathways is a series of subsequent generations. Figure 4 illustrates the procedure for four pathways; the circles denote the chosen starting points where on each *n*th generation path a new $(n + 1)$th generation path branches off. On a certain pathway, the time between its own starting point and the starting point of the next pathway, varied between 0.29 and 0.58 ps, which is in a sense the time that the system is allowed to relax on a pathway before a next generation one branches off.

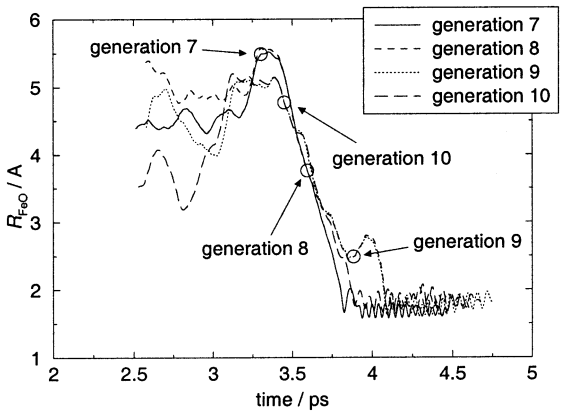

Figure 4. R_{FeO} during the last four reaction pathways from sequence B, with their starting points denoted by the circles. That is, pathway no. 7 was generated by simulating backward and forward in time starting from the configuration at $t = 3.303$ ps of pathway no. 6. The configuration at pathway 7 at $t = 3.594$ ps, was the starting configuration of pathway 8, et cetera. Note the shorter Fe^{IV}═O distance in pathway no. 7 (at about $t = 4$ ps) compared to the Fe^{IV}−OH distance in the later pathways.)

We calculated two sequences (sequence A and sequence B), each with a length of 10 generations. For the first generation of each sequence we took one of the 20 trajectories calculated earlier to verify the transition state location on the initial reaction pathway, shown in the right-hand-side plots of Figure 3. That is, the first generation pathways for both sequences A and B branch off at the transition state point of our initial pathway, with random atomic momenta drawn from a $T = 300$ K Boltzmann distribution. Of course, Figure 3 shows only halves of reactive pathways (namely from the TS point to either the product state or the reactant state), so the other half was calculated, for our two first generations, by integrating the equations of motion backward in time from the starting configuration of the reactive pathway (i.e., the TS point).

In Table 2, which shows some characteristics of the computed pathways for sequence A (first 11 rows) and sequence B (last 9 rows), we see that the first generation pathways of sequences A and B are quite different from each other. For sequence A, the pathway does not show the direct mechanism of our initial pathway in which the ferryl ion ($Fe^{IV}O^{2+}$) is formed via a rebound of the leaving $OH^{\bullet}$ radical, which abstracts the hydrogen of the intermediate Fe^{III}−OH. Instead, the leaving $OH^{\bullet}$ radical jumps after a lifetime of $\tau_{OH^{\bullet}} = 149$ fs via two solvent water molecules and terminates at a water ligand of a periodic image of the iron complex in a neighboring copy of the unit cell to form the dihydroxoiron(IV) moiety. This is indeed the first step of the two-step mechanism that we have seen before in

TABLE 2: Compilation of the Characteristics of the Reaction Paths Generated in Sequences A and B[a]

generation	mechanism	$\tau_{OH^\bullet}$/fs	# H_2O in H-bond wire	terminating Fe complex	final obs. species
		Relaxation Sequence A			
1	long wire	149	2	copy	ferryl
2	long wire	380	2	copy	ferryl
3	short wire	322	0	same	ferryl
5[b]	long wire	289	2	copy	$Fe^{IV}(OH)_3$
6	long wire	265	2	copy	$Fe^{IV}(OH)_3$
7	long wire	150	3	copy	ferryl
7	short wire	70	1	same	ferryl
8	short wire	73	1	same	$Fe^{IV}(OH)_3$
9	short wire	70	1	same	$Fe^{IV}(OH)_2$
9	short wire	65	1	same	$Fe^{IV}(OH)_3$
10	short wire	66	1	same	$Fe^{IV}(OH)_3$
		Relaxation Sequence B			
1[c]	both	101	2	both	ferryl
2	direct	121	0	same	ferryl
3	direct	133	0	same	ferryl
5[b]	direct	251	0	same	ferryl
6	direct	248	0	same	ferryl
7	direct	141	0	same	ferryl
8	long wire	43	2	copy	$Fe^{IV}(OH)_3$
9	long wire	42	2	copy	$Fe^{IV}(OH)_3$
10	short wire	93	1	same	$Fe^{IV}(OH)_3$

[a] The $O^\beta H^\bullet$ radicals formed in the paths of the first generations have relatively long lifetimes $\tau_{OH^\bullet}$. In sequence A already from the first generation no direct (i.e., rebound) mechanism is observed, but in the first generations, until generation 7 (except for generation 3) the H abstraction takes place along a long wire to the next box, to a water ligand of the periodic "copy" complex to form dihydroxoiron(IV) (and ferryl ion in the second step). The $O^\beta H^\bullet$ radicals in later generation paths of sequence A live shorter and terminate via a short wire at an aqua ligand of the initial iron complex ("same"). In the second step the acidic dihydroxoiron(IV) species can transform into a trihydroxo species or a ferryl ion (last column). In generations 1−7 of sequence B the $O^\beta H^\bullet$ radical abstracts the $O^\alpha H$ hydrogen to form the ferryl ion in one step (direct mechanism). Only in the later generations the transition paths relaxes to the abstraction through a H-bond wire, either a long wire (generations 8 and 9) or finally (generation 10) a short one. [b] Accidentally, for both sequences the 4*th* generation path was rejected because it recrossed from products to products, but was still used to generate a successful 5*th* generation reaction path. [c] The $O^\beta H^\bullet$ radical grabs simultaneously H^α and initiates an (unsuccessful) shunt to a periodic copy of the iron complex. See also text.

simulations starting from hydrogen peroxide already coordinated to pentaaquairon(II).[8,9] In a second step (see last column in Table 2), the ferryl ion was formed by donation of a proton by one of the hydroxo ligands to the solvent. For sequence B, the first generation pathway shows the rebound mechanism, although also an incipient $OH^\bullet$ radical shunt via two solvent water molecules is observed, but this $OH^\bullet$ shunt is not completed, the motion of the solvent hydrogens is reversed when the Fe^{III}−OH intermediate donates its hydrogen to the leaving $OH^\bullet$ radical.

From these two first generation pathways, we successively generated new pathways by taking a configuration from a path and changing the atomic momenta. The momenta were changed by randomly drawing new momenta from a Gaussian distribution of $T = 5$ K or $T = 10$ K and adding these to the old momenta (and correcting for any total momentum of the system). The success rate of obtaining a new pathway connecting reactants and products was about 50%. In both sequences, accidentally, the fifth generation pathway was started from an unsuccessful fourth generation pathway that started in the product well and recrossed back to the product well, although the iron−oxygen distances reached a separation of more than 4 Å (which is our order parameter defining the reactant well) in both fourth generation pathways.

Taking a closer look at Table 2, we see trends along the two sequences which could indicate that indeed our initial pathway is an atypical one and relaxation toward more representative pathways does take place. For example, the time that the leaving $OH^\bullet$ radical remains intact before abstracting a hydrogen from the complex or a solvent water (the lifetime $\tau_{OH^\bullet}$, which is measured from the moment of O−O lysis, defined as $R_{OO} > 2.0$ Å, until the first H-abstraction by $OH^\bullet$), is seen to decrease in both sequences. Second, in both sequences the followed mechanisms change via or from the "long-wire two-step" mechanism (in which the $OH^\bullet$ radical in the first step terminates via a wire of two or three solvent waters at a water ligand of the periodic image of the complex) to the "short-wire two-step" mechanism. In the latter case, the leaving $OH^\bullet$ radical terminates in the first step at an adjacent water ligand (thus stays in the same unit cell) via one bridging solvent molecule, forming the dihydroxoiron(IV) complex. Figure 5 shows in four snapshots the H_2O_2 coordination to iron(II), the O−O lysis, and the $OH^\bullet$ radical shunt and termination of such a short-wire step. In fact, this new "short-wire" reaction pathway was already predicted in previous work where we discussed the possibilities for a radical shunt in a very large box containing a single pentaaquairon(II)−hydrogen peroxide complex.[8] In our present pathway relaxation procedure it indeed appears spontaneously.

The last column in Table 2 displays the last observed iron complex. It shows that not always is the ferryl ion formed, but instead in many cases an $[Fe^{IV}(H_2O)_3(OH)_3]^+$ complex. This is due to the dynamic equilibrium between the acidic dihydroxo species and its conjugate base, the hydrolyzed trihydroxo species, by proton donation to the solvent:

$$[(H_2O)_4Fe^{IV}(OH)_2]^{2+} + H_2O \leftrightarrow [(H_2O)_3Fe^{IV}(OH)_3]^+ + H_3O^+ \quad (4)$$

Formation of the ferryl ion by H-donation of one of the dihydroxo ligands to the solvent is only favorable if the system finds itself on the left-hand-side of eq 4. Most reaction pathways are however too short to observe the ferryl ion formation as the second step.

VI. Discussion

The pathway relaxation from an artificially constructed reaction pathway to a pathway without the memory of the initial construction, was obtained in two steps (for both sequences A and B). The first step took place in the first pathway generation, namely by taking completely random atomic momenta at the starting point (which was the transition state configuration of the initial reaction pathway). The second part of the relaxation consisted of nine more sequential pathway generations, in which we observed (a) increasingly faster terminations of the leaving $OH^\bullet$ radical due to shorter lifetimes $\tau_{OH^\bullet}$ and (b) a shift from the direct rebound mechanism and the long-wire two-step mechanism to the short-wire two-step mechanism.

These changes along the two sequences of pathways can be understood as the result of the relaxation of the solvent environment of the reactants. As an illustration, Figure 6 shows the hydrogen−oxygen distances $R_{O^\beta H}$ as a function of time for the solvent water hydrogens within a radius of 2 Å of the H_2O_2 oxygen, O^β, for the initial unrelaxed reaction pathway (upper graph) and the last pathway (no. 10) of sequence A (lower graph). The moment that the hydrogen peroxide O−O distance equaled $R_{OO} = 2.00$ Å, which marks the moment of coordination and dissociation of the hydrogen peroxide to the iron complex, was taken for time $t = 0$, marked by the vertical dashed line.

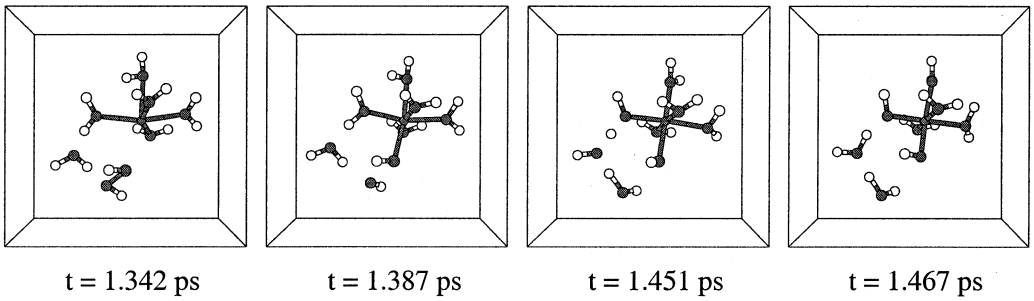

Figure 5. Four snapshots of the 10th generation reaction path of sequence A, which had a total length of 2.68 ps, showing the formation of the dihydroxoiron(IV) complex by H-abstraction from an H_2O ligand by the leaving $OH^\bullet$ radical via one bridging solvent water molecule. The bridging solvent molecule which is H-bonded to H_2O_2 from $t = 0$ ps is also shown, but for simplicity, the other solvent water molecules are left out.

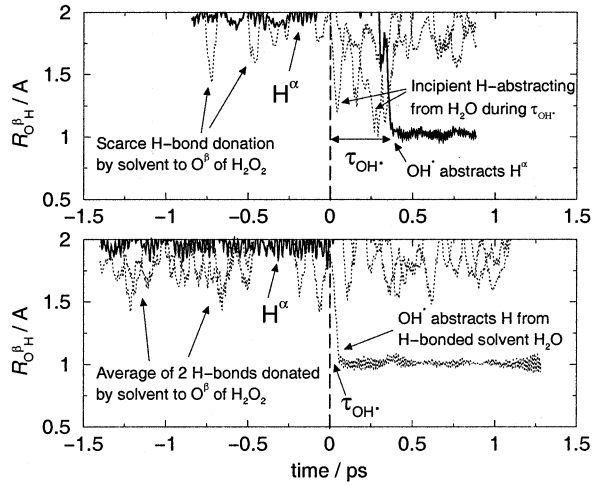

Figure 6. Distances between solvent hydrogens and O^β (the hydrogen peroxide oxygen not bonded to iron) during the unrelaxed initial pathway (upper graph) and the last pathway of sequence A (lower pathway). The increased number of hydrogen bonds in the latter, especially before $t = 0$ (the moment of dissociation defined as $R_{OO} = 2.00$ Å) indicates the intended solvent relaxation.

Before $t = 0$, we see the lines arising from the hydrogen-bonded solvent water molecules to the yet intact hydrogen peroxide and from the H_2O_2 hydrogen H^α (distinguished by the bold line in the graphs). The $R_{O^\beta H^\beta}$ distance, fluctuating around 1 Å has been left out for clarity. After $t = 0$, we see the lines arising from the hydrogen-bonded solvent water molecules to the, at first, leaving $OH^\bullet$ radical and later formed water molecule oxygen. Note that the change from $OH^\bullet$ radical into water molecule occurs almost 300 fs later in the initial pathway compared to the relaxed pathway and that the $OH^\bullet$ abstracts H^α (from the formed $Fe^{III}-OH^\alpha$) in the initial pathway but in the relaxed pathway it abstracts the hydrogen from one of the hydrogen-bonded solvent molecules. Also, we see in the upper graph of the unrelaxed pathway jumps from two solvent hydrogens to the $OH^\bullet$ radical between $t = 0-0.35$ ps, which however do not make it to a H atom at the water molecule that is formed; this is "achieved" by the H^α.

The initial reaction pathway was constructed by driving hydrogen peroxide out of the coordination shell from the $[Fe^{II}(H_2O)_5(H_2O_2)]^{2+}$ complex, as shown earlier in Figure 1 between $t = 5.1-5.7$ ps. We thus started from H_2O_2, separated from the complex, that could hardly have formed a relaxed solvation shell, which however is expected to exist for separated reactants in the reactant well. This is seen in the upper graph of Figure 6 from the absence of hydrogen bonds from solvent waters before $t = 0$. The lower graph, of reaction pathway no. 10, on the other hand, shows two solvent hydrogens with $R_{O^\beta H}$ distances between 1.5 and 2.0 Å,[29] indicating the adoption of hydrogen bonds from the solvent network and thus indicating that relaxation of the solvent structure has occurred around hydrogen peroxide. Because hydrogen peroxide takes part in the three-dimensional solvent network via the formed hydrogen bonds between solvent molecules and H_2O_2 before the reaction with iron (which is also illustrated in the first snapshots in Figure 5) the leaving $OH^\bullet$ radical can terminate much faster via H-bond wires in the network, resulting in the lower lifetime $\tau_{OH^\bullet}$.

Have we now found the most likely mechanism for the iron(II)-catalyzed dissociation of hydrogen peroxide? Let us first consider the alternative to the proposed two-step mechanism, namely the rebound mechanism. Of course, whether the two-step mechanism is indeed more favorable than this alternative can in principle be established only after generating a very large number of independent iron reaction pathways, and compare the probabilities of the two mechanisms. Our transition path sampling sequences indicate the rebound mechanism to have lower probability than the two-step mechanism. This can be rationalized from the following motive. In the rebound mechanism, the leaving $OH^\bullet$ has to abstract the $Fe^{III}-OH^\alpha$ hydrogen. From our results, however, we see that the leaving $OH^\bullet$ from the solvated hydrogen peroxide will jump rapidly along an H-bond wire to termination, which is much more probable, simply because the $Fe^{III}-OH^\alpha$ hydrogen is further away after the O−O lysis than the solvent molecules forming H-bonds.

The alternative mechanism to the two aforementioned ones (with a ferryl ion as the active intermediate) is Haber and Weiss' free radical mechanism. We have given arguments in refs 8, 9, and 14 why we believe this mechanism to be unlikely. If we would still want to compare its probability to that of the two-step (ferryl ion producing) mechanism, we should consider that for the Haber and Weiss radical mechanism, the leaving $OH^\bullet$ radical has to become a "free radical" by jumping along an H-bond wire of a number of solvent waters. The $OH^\bullet$ then should become disconnected, possibly by a thermal rotation of one of the involved solvent waters, so that the $OH^\bullet$ radical cannot jump back to terminate at the aquairon complex. In our rather small system, the occurrence or nonoccurrence of the latter event cannot be adequately tested since an $OH^\bullet$ radical that leaves the complex to become a free radical via a short wire of, say, three solvent waters, is already too close to the periodic image of the iron complex at which it can terminate. For reaction path sampling of the Haber and Weiss free radical mechanism, a larger unit cell would be essential.

Let us finally note that the AIMD simulations are not without shortcomings. The box size was chosen rather small in order to make the computations feasible. The $OH^\bullet$ radical could therefore jump via a hydrogen-bonded wire of three water molecules through the unit cell to a neighboring periodic copy of the cell.

So, although the reactants have at least one complete hydration shell, and the major solvation contributions are included in the calculations, the long-range effects are approximated and the simulations can, in the future when computers become faster, be improved by increasing the box size and the number of solvent molecules in the box. Other (minor) error sources are the neglect of pressure effects in the NVT ensemble, the classical treatment of the nuclear dynamics neglecting tunneling and zero-point energy effects, and the accuracy of electronic structure method which is with the present exchange-correlation functions of DFT about 1 kcal/mol, and significantly larger (due to approximations in the PAW method) when changes in oxidation state of the metal are involved, see Section III.

VII. Conclusion

We have successfully applied the reaction path generation technique used in transition path sampling in order to obtain relaxed reaction pathways of the reaction between pentaaquairo-n(II) and hydrogen peroxide in aqueous solution. The initial reaction pathway which was the subject of this relaxation procedure showed a rebound mechanism in which the hydrogen peroxide O−O bond dissociated at H_2O_2 coordination to the iron(II) center, after which the leaving $OH^{\bullet}$ radical rebounded to abstract the intermediate Fe^{III}−OH hydrogen, forming the ferryl ion and a water molecule. We generated two sequences of 10 reaction pathways from this initial path in order to obtain pathways which have lost the memory of the artificial construction of the initial pathway. Along these sequences, we found a shift to a new mechanism in which the leaving $OH^{\bullet}$ jumps via a solvent water molecule and abstracts the hydrogen from a water ligand forming a dihydroxoiron(IV) complex and a water molecule. The mechanistic change can be rationalized as the result of the proper reestablishing of the solvent structure around the reactants, which had been broken up in the artificial generation of the initial pathway. It is to be noted that the "mechanism" which emerges from these transition path sampling experiments is precisely the one found in our earlier AIMD simulation, starting from coordinated H_2O_2,[15] and was indeed already indicated by gas-phase calculations.[14]

Acknowledgment. We acknowledge gratefully the support by the Prioriteits Programma Materialen−Computational Materials Science (PPM-CMS). We thank the foundation NCF of The Netherlands Foundation of Scientific Research (NWO) for computer time.

References and Notes

(1) Mohr, M.; Marx, D.; Parrinello, M.; Zipse, H. *Chem. Eur. J.* **2000**, *6*, 4009.
(2) Aagaard, O. M.; Meier, R. J.; Buda, F. *J. Am. Chem. Soc.* **1998**, *120*, 7174.
(3) Mann, D. J.; Hase, W. L. *Phys. Chem. Chem. Phys.* **2001**, *3*, 4376.
(4) Yoshizawa, K.; Shiota, Y.; Kagawa, Y.; Yamabe, T. *J. Phys. Chem. A* **2000**, *104*, 2552.
(5) Van Speybroeck, V. Theoretische studie van chemische reacties met statische en dynamische ab initio methoden. Thesis, Universiteit Gent, Belgium, 2001, Chapter 8.
(6) Dellago, C.; Bolhuis, P. G.; Csajka, F. S.; Chandler, D. *J. Chem. Phys.* **1998**, *108*, 1964.
(7) Bolhuis, P. G.; Dellago, C.; Chandler, D. *J. Chem. Phys.* **1998**, *108*, 9236.
(8) Ensing, B.; Buda, F.; Blöchl, P. E.; Baerends, E. J. *Angew. Chem., Int. Ed.* **2001**, *40*, 2893.
(9) Ensing, B.; Buda, F.; Blöchl, P. E.; Baerends, E. J. *Phys. Chem. Chem. Phys.* **2002**, *4*, 3619.
(10) Fenton, H. J. H. *J. Chem. Soc.* **1894**, *65*, 899.
(11) Haber, F.; Weiss, J. *Proc. R. Soc. London* **1934**, *147*, 332.
(12) Bray, W. C.; Gorin, M. H. *J. Am. Chem. Soc.* **1932**, *54*, 2124.
(13) Geissler, P. L.; Dellago, C.; Chandler, D.; Hutter, J.; Parrinello, M. *Sci.* **2001**, *2121*, 291.
(14) Buda, F.; Ensing, B.; Gribnau, M. C. M.; Baerends, E. J. *Chem. Eur. J.* **2001**, *7*, 2775.
(15) Ensing, B.; Meijer, E. J.; Blöchl, P. E.; Baerends, E. J. *J. Phys. Chem. A* **2001**, *105*, 3300.
(16) Meijer, E. J.; Sprik, M. *J. Phys. Chem. A* **1998**, *102*, 2893.
(17) Meijer, E. J.; Sprik, M. *J. Am. Chem. Soc.* **1998**, *120*, 6345.
(18) Car, R.; Parrinello, M. *Phys. Rev. Lett.* **1985**, *55*, 2471.
(19) Parr, R. G.; Yang, W. *Density-Functional Theory of Atoms and Molecules*; Oxford University: New York, 1989.
(20) Becke, A. D. *Phys. Rev. A* **1988**, *38*, 3098.
(21) Perdew, J. P. *Phys. Rev. B* **1986**, *33*, 8822.
(22) Blöchl, P. E. *Phys. Rev. B* **1994**, *50*, 17953.
(23) Baerends, E. J.; Ellis, D. E.; Ros, P. *Chem. Phys.* **1973**, *2*, 41.
(24) Chong, D. P. Private communication: high-quality even-tempered all-electron STO basis sets.
(25) Nosé, S. J. *J. Chem. Phys.* **1984**, *81*, 511.
(26) Geissler, P. L.; Dellago, C.; Chandler, D. *J. Phys. Chem. B* **1999**, *103*, 3706.
(27) Dellago, C.; Bolhuis, P. G.; Chandler, D. *J. Chem. Phys.* **1999**, *110*, 6617.
(28) Swift, T. J.; Connick, R. E. *J. Chem. Phys.* **1962**, *37*, 307.
(29) The average H-bond length in liquid water was earlier estimated to be 1.73 Å from the radial distribution functions obtained with AIMD simulations in ref 15.